Multipoint measurements employing a microwave interferometer and a Langmuir probe in the detached linear plasma

Cite as: AIP Advances **9**, 015016 (2019); https://doi.org/10.1063/1.5081929
Submitted: 18 November 2018 . Accepted: 07 January 2019 . Published Online: 16 January 2019

H. Natsume, H. Tanaka, S. Kajita, M. Yoshikawa, M. Seki, H. Ohshima, and N. Ohno

Multipoint measurements employing a microwave interferometer and a Langmuir probe in the detached linear plasma

Cite as: AIP Advances 9, 015016 (2019); doi: 10.1063/1.5081929
Submitted: 18 November 2018 • Accepted: 7 January 2019 •
Published Online: 16 January 2019

H. Natsume,[1,a)] H. Tanaka,[2] S. Kajita,[2] M. Yoshikawa,[3] M. Seki,[1] H. Ohshima,[1] and N. Ohno[1]

AFFILIATIONS

[1]Graduate School of Engineering, Nagoya University, Furo-cho, Chikusa-ku, Nagoya 464-8603, Japan
[2]Institute of Materials and Systems for Sustainability, Nagoya University, Furo-cho, Chikusa-ku, Nagoya 464-8603, Japan
[3]Plasma Research Center, University of Tsukuba, 1-1-1 Tennodai, Tsukuba, Ibaraki 305-8577, Japan

[a)]Electronic mail: natsume.hiroki@d.mbox.nagoya-u.ac.jp

ABSTRACT

Multipoint measurements were carried out by employing a microwave interferometer (MI) and a Langmuir probe (LP) in steady-state detached plasmas in the linear plasma device NAGDIS-II to reveal the structure of fluctuations along the magnetic field. We changed the LP position along the magnetic field while the MI was fixed at an upstream position. In addition, a fast framing camera was used to identify an azimuthal mode number, and the predominant mode number was identified as $m = 1$. By analyzing correlations between signals observed by the LP and the MI, it was found that a time delay of 10–20 kHz fluctuations gradually decreased toward the downstream direction. The results indicate a decrease in the rotation velocity in the $E \times B$ direction, and suggest that the 10–20 kHz fluctuation forms a spiral shape.

I. INTRODUCTION

In magnetic confinement fusion reactors such as ITER and DEMO, it is necessary to minimize the damage to the plasma-facing components caused by the plasma flowing out from the core region. In the divertor configuration, in order to accomplish this, the particle flux and the heat flux are led to the divertor region. However, unless countermeasures are adopted, the divertor target will be exposed to a thermal load of several tens of MW/m^2, which greatly exceeds the allowable thermal load of the materials. Therefore, reduction of the heat load to the divertor target is important for the implementation of nuclear fusion reactors.

As a method for reducing the thermal load of the divertor region, detached plasma is effective.[1] In this method, by increasing the neutral gas pressure, the plasma is neutralized in front of the divertor target by the plasma recombination process. At this time, in addition to the heat flux, the particle flux to the divertor target decreases, and then the thermal load decreases greatly.[2] The simulation of detached plasma still experiences difficulties in reducing the ion particle flux to the same degree as the actual experimental.[3] This may possibly be due to the fact that, in addition to the volume recombination, the plasmas are transported in the cross-field direction. When the divertor was detached, a flattening of an electron density profile in the scrape-off layer happened and was explained as an increase in the cross-field transport.[4,5] Furthermore, around the detached plasmas in several toroidal devices[6–8] and linear devices,[9,10] enhanced cross-field transports were observed. However, the phenomenon is insufficiently understood, and detailed investigations are needed to improve the accuracy of the simulation.

In the linear device NAGDIS-II, in the vicinity of the recombination front where strong gradients of plasma parameters existed, large electron density fluctuation and an axially local increase in radial plasma ejection have been

observed.[11,12] A fast framing camera measurement, which captured line-of-sight signals along the magnetic field, clarified that the ejected plasma transported in the periphery forms a spiraling structure rotating in the E × B drift direction.[13] Further, the dominant azimuthal mode numbers are identified as m = 1 and 2. From past research, however, the phase relationship of the plasma structure along the magnetic field has not yet been clarified. Therefore, we investigated the phase relationship of fluctuations along the magnetic field in this study.

We carried out multipoint measurements employing a microwave interferometer (MI)[14] and a Langmuir probe (LP) in the steady-state detached plasma, and changed the measurement position of the LP at equal intervals in the direction of the magnetic field. Correlation analysis was applied to the ion saturation current (I_{sat}) fluctuation obtained at each point and the line-integral electron density (n_{el}) fluctuation of the MI. In order to identify the azimuthal mode number m, correlation analysis was also applied to the emission intensity signal observed from the side of the vessel with the fast framing camera. Consequently, a time delay in the fluctuation between two distant locations was found. Moreover, we discussed fluctuation behaviors along the magnetic field in the detached plasma.

In the following section, the experimental setup in NAGDIS-II will be explained. Analyses and the results will be shown in Sec. III. A discussion of the results and concluding remarks will be given in Sec. IV and V, respectively.

II. EXPERIMENTAL DEVICES AND MEASUREMENTS

The parameter measurement was conducted in the linear plasma device NAGDIS-II, which can generate a cylindrical steady-state helium plasma by a DC discharge.[15] As shown in figure 1(a), NAGDIS-II has a cylindrical vacuum chamber with a length of ~2.5 m including the discharge region and the test region. The radius of the test region is 90 mm. A detach plasma is easily produced by increasing the neutral gas pressure around the end target in this device. The gas pressures, p1 and p2, were measured by Baratron vacuum gauges at mid-stream and downstream, respectively. The operation conditions in this study are summarized in Table I.

TABLE I. Operation conditions.

Parameters	Parameters
Discharge current	20 A
Discharge voltage	120 V
Magnetic field	0.1 T
Mid-stream gas pressure	7.3 mTorr
Downstream gas pressure	7.8 mTorr

We investigated the structure of fluctuation along the magnetic field by employing the MI and the LP. The two measurements simultaneously sampled plasma properties at a sampling frequency of 1 MHz.

The 70.15 GHz MI obtained the upstream n_{el} fluctuation without disturbances. As shown in figure 1(a), the MI was fixed at z = 0 mm (660 mm upstream from the end target). The microwave passed through the plasma column at y = 20 mm from the plasma center in the $-x$ direction. Strong emission from near the recombination front was further upstream from the position of the MI, according to spectrometry. The electromagnetic wave was the O wave, and the cut-off frequency, n_c, was 6.1×10^{19} m^{-3}, and is given by the following formula:

$$n_c = 126\pi^2 \times 10^{-5} f^2 \left[\mathrm{m}^{-3}\right]. \quad (1)$$

Its spatial resolution was a few centimeters in the radial direction.

We employed the LP to measure I_{sat} at downstream positions along the z direction. The ion saturation current and electron density, n_e, have the following relationship:

$$I_{sat} \propto n_e T_e^{1/2} \quad (2)$$

where T_e is the electron temperature. The LP enables two-dimensional measurement by insertion with the robot cylinder and rotation of the insertion rod, as shown in figure 1(b).

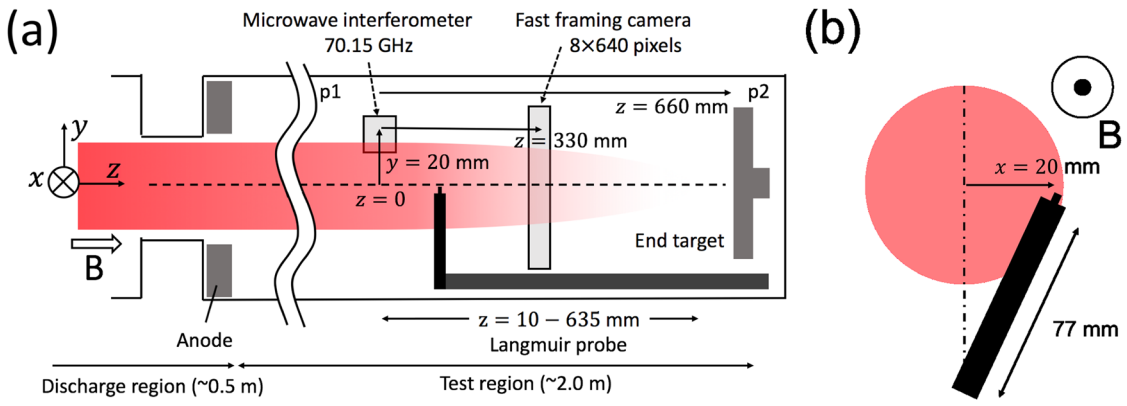

FIG. 1. (a) Schematic diagram of the experimental setup and (b) the radial position of the LP in NAGDIS-II.

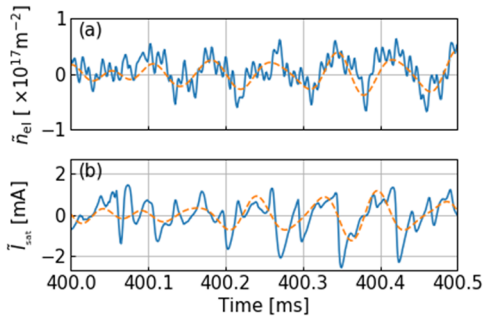

FIG. 2. Time series of the (a) $\tilde{n}_{el}$, (b) $\tilde{I}_{sat}$ (solid line) and those of 10–20 kHz components (dashed line).

Therefore, the LP can move in both directions, i.e., parallel and perpendicular to the magnetic field. In this study, the position of the LP was changed at intervals of 25 mm in the z direction within the range z =10–635 mm. The radial distance was fixed as 20 mm in the x direction.

We also applied the fast framing camera to identify an azimuthal mode number (m). The fast framing camera with a resolution of 8×640 was fixed at z = 330 mm. The frame rate was 87000 fps, the sampling period was ~11.5 μs, and the shutter speed was 9 μs.

III. ANALYSES AND RESULTS

Figures 2(a) and (b), respectively, show a time series of fluctuations (solid line) and 10–20 kHz components (dashed line) in n_{el} and I_{sat} when the LP was fixed at z = 10 mm. The two signals were measured at the same time, and it was confirmed that there was a phase difference between them. The fluctuation level in the $\tilde{n}_{el}$ appeared to be higher, because it included all fluctuations along the line of sight.

A. Frequency characteristics

In this section, the frequency characteristics of the fluctuations are investigated with Fourier analysis. Figure 3(a) exhibits the power spectral densities (PSDs) of n_{el} and I_{sat} fluctuations. It can be confirmed that there are spectral peaks between 10 and 20 kHz in both PSDs. It is likely that the 10–20 kHz fluctuation corresponds to azimuthal rotation, as will be discussed in Sec. III C. There is also a strong fluctuation in the low-frequency band (<4 kHz) in n_{el}, because it included some of the center fluctuation due to the spatial resolution of the MI. Figures 3(b) and (c) show a spectrogram and the statistical moments of I_{sat} as a function of the distance between the MI and the LP in the z direction, respectively. The peak between 10 and 20 kHz gradually decreases toward the downstream direction because of the detachment.

B. Correlation between two distant locations

Correlation analysis is widely used in the fusion plasmas and is a powerful tool for identifying a spatial-temporal behaviour.[16,17] In this section, we investigate the correlation between n_{el} and I_{sat} fluctuations by focusing on the 10–20 kHz frequency components. Thus, before the correlation analysis, a bandpass filter with a range of 10–20 kHz was applied to

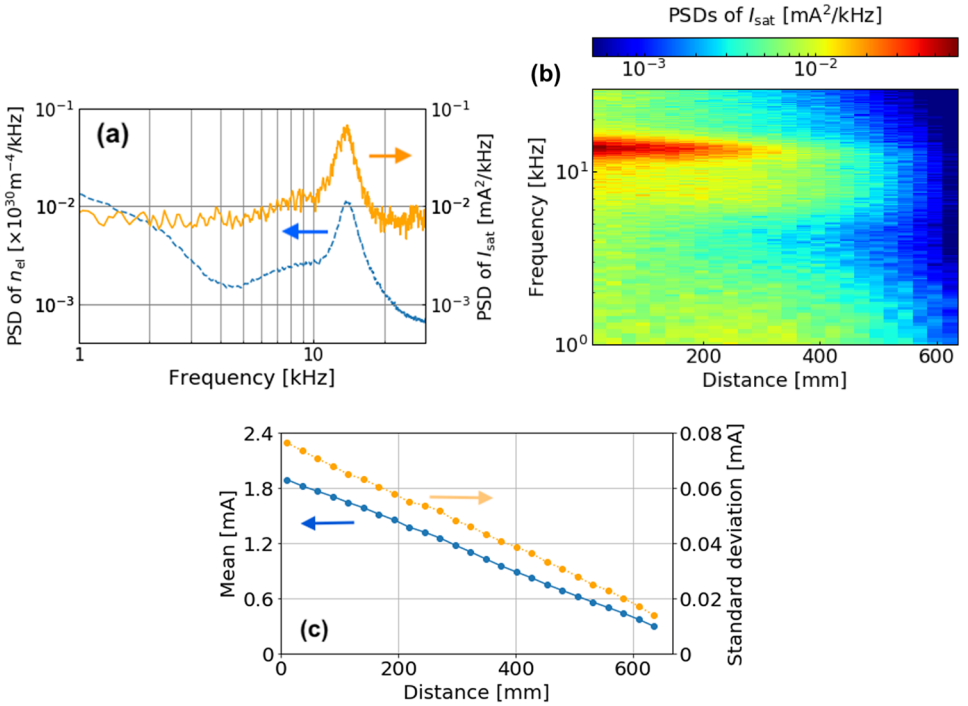

FIG. 3. (a) PSDs of n_{el} (dashed line) and I_{sat} (solid line) fluctuations as a function of frequency. (b) Spectrogram and (c) mean (solid line) and standard deviation (dashed line) of the I_{sat} as a function of the distance between the MI and the LP.

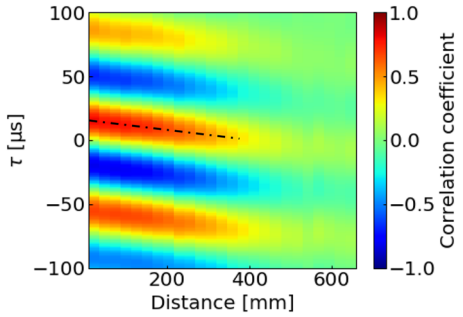

FIG. 4. Map of $R(n_{el}, I_{sat})$ as functions of the distance between the MI and the LP, and the time shift τ defined by Eq. (3).

these signals. The cross-correlation coefficient between the two signals $a(t)$ and $b(t)$ is defined by

$$R(a,b)(\tau) = \frac{\langle \tilde{a}(t)\tilde{b}(t+\tau)\rangle}{\sqrt{\langle \tilde{a}(t)^2\rangle}\sqrt{\langle \tilde{b}(t)^2\rangle}}. \quad (3)$$

The results of $R(n_{el}, I_{sat})$ at every position of the LP along the magnetic field are summarized in figure 4. It can be noticed that there is a temporal periodicity, and the peak magnitudes of $R(n_{el}, I_{sat})$ decrease toward the downstream direction. In addition, the drawn patterns fall downward to the right as illustrated by the dashed line. The intercept is ~15 μs and the slope is ~-0.04 μs/mm, which corresponds to a phase speed of 25 km/s.

C. Mode number identification

To identify an azimuthal mode number of the 10–20 kHz frequency components, we applied the correlation analysis to images of the visible light emission captured by the fast framing camera. We first averaged the emission intensity in the axial direction and obtained a 292-sized data array with 10^5 time frames. Before applying the correlation analysis, we extracted the 10–20 kHz frequency components by using a bandpass filter. Figure 5(a) shows a plot of the standard deviation of the 10–20 kHz frequency components of the emission intensity versus the y direction, E_y. In figure 5(a), peaks appear at y = ±10 mm.

Figure 5(b) shows $R(E_{10\,mm}, E_y)$, which is the correlation coefficients between $E_{10\,mm}$ and E_y. The auto-correlation coefficients are expressed by the dashed line. $R(E_{10\,mm}, E_y)$ was low around y = 0 mm, because the captured emission intensity was the line-integrated data in the x direction and canceled by the high-intensity and low-intensity components. It is confirmed that there are periodicities around ±10 mm, which have an anti-phase relationship.

Figures 5(c) and (d) show the time series of fluctuation components and filtered emission intensity signals plotted with solid and dashed lines at y = 10 mm and y = –10 mm, respectively. The two filtered emission intensity signals had an anti-phase relationship. Because m = 1 and 2 modes were dominant in NAGDIS-II,[13] it can be concluded that the azimuthal

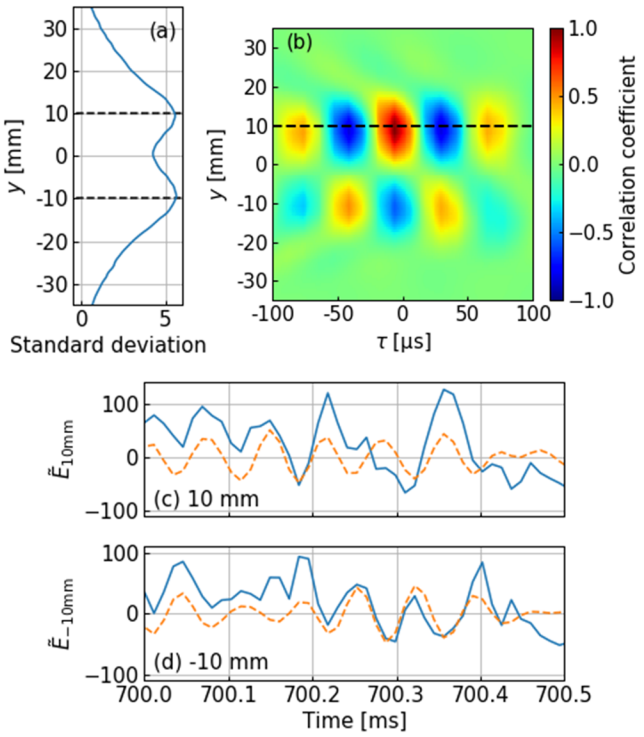

FIG. 5. (a) Standard deviation of the 10–20 kHz components of emission intensity signals, (b) map of $R(E_{10\,mm}, E_y)$ as a function of y and the time shift τ defined by Eq. (3), and (c) raw time series of the emission intensity signal (solid line) and 10–20 kHz components (dashed line) at y = 10 mm and (d) at y = –10 mm. y was measured from the highest emission intensity position.

mode number of the 10–20 kHz frequency components was m = 1.

IV. DISCUSSION

Because the fluctuation rotated with m = 1 in the E × B direction, i.e., in the counterclockwise direction in figure 1(b), the time delay between n_{el} and I_{sat} can transform into a phase difference. For example the phase difference became ~90° the LP was at z = 10 mm, which coincided with the positional relation in the MI and the LP, because the time delay was ~15 μs and the rotation period T ~60 μs.

The rotation velocity, v_{rot}, was estimated to be ~2.1 km/s by using the relation $v_{rot} = 2\pi mr/T$, where r is the radius. On the other hand, the ion sound speed, C_s, was estimated to be in the range 2.2–2.7 km/s by using the electron temperature measured by the double-probe method at x = 20 mm. Because the Mach number, M_c, in detached plasmas was ~0.4 in NAGDIS-II,[18] the parallel flow $v_{\parallel} = M_c C_s$ was comparable to or less than v_{rot}. In Sec. III B, the phase speed was estimated at 25 km/s, which is much greater than $v_{\parallel}$ and v_{rot}. We interpret the determination of the phase speed below.

One possible reason for the above phase speed estimation result is that an instability generating the plasma

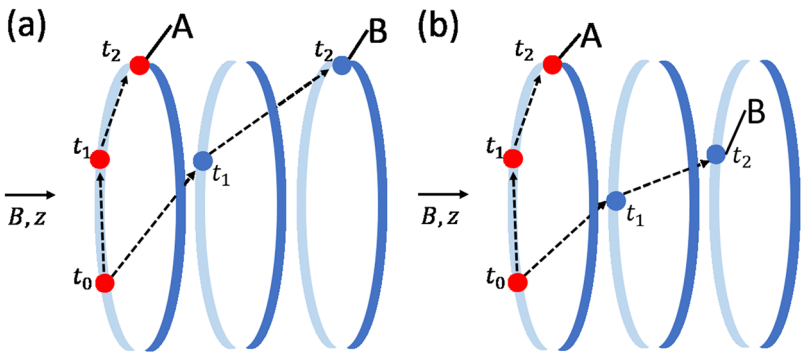

FIG. 6. (a) Schematic diagram of time traces of azimuthal positions of the two types of ejected plasmas with the constant $E \times B$ drift speed and (b) decreasing the $E \times B$ drift speed.

ejection has an azimuthal phase shift along z. However, from past research,[11,19] the ejecting region would be localized in the z direction around the recombination front, which was further upstream from the measuring position in this study. In such a case, the phase shift shown in figure 4 could be explained as follows.

Figure 6 illustrates the time traces of azimuthal positions of the two types of ejected plasmas. One does not move along z after the ejection (A in figure 6). The other moves along z with a parallel speed of $v_{\parallel}$ (B in figure 6). Due to the radial electric field, they rotate in the azimuthal direction by the action of the $E \times B$ drift. If the $E \times B$ drift speed were constant along z, the phase difference between them would always become zero in the azimuthal direction, as illustrated in figure 6(a). However, the $E \times B$ drift speed would not be constant in the detached plasmas. Because T_e decreases along the magnetic field toward the end target because of the detachment, the magnitude of the space potential, $|V_s|$, could become small. The space potential at each position is calculated by $V_f + 3.7T_e$ where V_f is a floating potential. Radial distributions of V_s at several z positions are shown in figure 7. Its gradient in the range 10–20 mm in the radial direction surely becomes smaller as the increment in z direction. Thus, the $E \times B$ rotation speed becomes small with increasing z, as illustrated in figure 6(b). In this case, a phase delay would occurs that coincides with figure 4. As a result, the fluctuation component would form a spiral shape that rotates in the $E \times B$ direction.

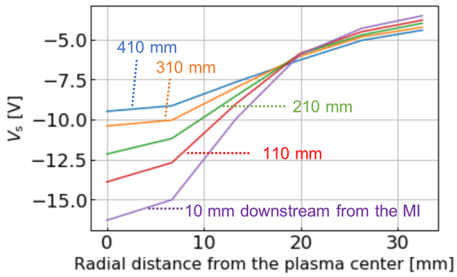

FIG. 7. Space potential at several z positions.

V. CONCLUSION

In order to clarify the structure of the fluctuation along the magnetic field, we have conducted multipoint measurements with a microwave interferometer and Langmuir probe in NAGDIS-II. Applying spectral and correlation analysis techniques, we found that the 10–20 kHz fluctuation propagated toward the downstream direction with a time delay while rotating azimuthally with mode number m = 1. The time delay decreased linearly with increasing distance between the microwave interferometer and the LP along the magnetic field. A possible reason for this is that the rotation velocity in the $E \times B$ direction gradually decreased with axial distance because of the decrease in the temperature. Further, the results suggest that the 10–20 kHz fluctuation forms a spiral shape rotating in the $E \times B$ direction.

Because the measurements in this study were performed further downstream from the recombination front, it would be interesting to employ the recombination front from upstream to downstream. We are planning to investigate fluctuation behaviors in detail in the vicinity of a recombination front with this system in the near future.

ACKNOWLEDGMENTS

This work was supported by JSPS KAKENHI (16H06139, 16H02440), NIFS Collaboration Research program (NIFS17KUGM130, NIFS17KUGM120), and NINS program of Promoting Research by Networking among Institutions (01411702). We would like to thank Editage (www.editage.jp) for English language editing.

REFERENCES

[1] P. C. Stangeby, *The Plasma Boundary of Magnetic Fusion Devices* (Institute of Physics Publishing, Bristol, 2000).
[2] M. Shimada *et al.*, J. Nucl. Mater. **111-121**, 362 (1982).
[3] K. Hoshino *et al.*, J. Plasma Fusion Res. Series **9**, 592 (2010).
[4] H. J. Sun *et al.*, Plasma Phys. Control. Fusion **57**, 125011 (2015).
[5] D. Carralero *et al.*, Nucl. Fusion **58**, 096015 (2018).
[6] B. Stansfield *et al.*, J. Nucl. Mater. **241-243**, 739 (1997).
[7] S. Potzel *et al.*, J. Nucl. Mater. **438**, S285 (2013).
[8] H. Tanaka *et al.*, Phys. Plasmas **17**, 102509 (2010).
[9] N. Ohno *et al.*, J. Plasma Fusion Res. **80**, 275 (2004).

[10]E. M. Hollmann *et al.*, Phys. Plasmas **8**, 3314 (2001).
[11]K. Takeyama *et al.*, Plasma Fusion Res **12**, 1202007 (2017).
[12]H. Tanaka *et al.*, Plasma Phys. Control. Fusion **60**, 075013 (2018).
[13]H. Tanaka *et al.*, Contrib. Plasma Phys **50**, 256–266 (2010).
[14]M. Yoshikawa *et al.*, Plasma Fusion Res. **10**, 1202088 (2015).
[15]N. Ohno *et al.*, Nucl. Fusion **41**, 1055 (2001).
[16]O. Grulke *et al.*, Phys. Plasmas **13**, 012306 (2006).
[17]S. Inagaki *et al.*, Plasma Fusion Res. **6**, 1402017 (2011).
[18]E.-K. Park *et al.*, Curr. Appl. Phys. **12**, 1497 (2012).
[19]Y. Hayashi *et al.*, Phys. Plasmas **23**, 012511 (2016).